Mem. S.A.It. Vol. 7, 48

Memorie della
Supplementi

Gravitational microlensing effects on the broad emission lines of quasars

C. Abajas[1] , E. Mediavilla[1], J.A. Muñoz[2] and L. Č. Popović[3]

[1] Instituto de Astrofísica de Canarias, C/Vía Láctea, 38205 La Laguna, Tenerife, Spain.
[2] Departamento de Astronomía y Astrofísica, Universidad de Valencia, 46100 Burjassot, Valencia, Spain.
[3] Astronomical Observatory, Volgina 7, 11160 Belgrade, Serbia. e-mail: abajas@iac.es, emg@iac.es, jmunoz@uv.es, lpopovic@aob.bg.ac.yu

Abstract. Multiple images of QSOs are formed when the gravitational field of an intervening galaxy bends the trajectories of the light rays. The granulation of the lens galaxy mass distribution (either in stars or compact dark matter objects) could induce non correlated variability between different images of the lensed QSO (microlensing). The relevance of microlensing depends on the source size and, on light of some recent results, could affect to the Broad Emission Lines of QSOs. In this contribution we review the effects on the BLR of microlensing by an isolated microlens, a straight fold caustic and a caustic network.

Key words. Cosmology: gravitational lensing – quasar: emission lines – quasar:individual: Q2237+0305

1. Introduction

The standard model states that a QSO has a massive black hole in the centre with an accretion disk around, where the UV continuum is generated. This central engine is surrounded by ionized gas clouds moving with high velocities. The UV continuum region has a size around 0.001pc, and it was thought that the ionized clouds region producing the broad emission lines (BEL) had a radius between 0.1 and 1 pc (Rees 1984).

The amplification produced by a gravitational lens (GL) depends on the ratio between the sizes of extended object and the Einstein radius, η_0, associated with the lens, being smaller sources which will experience larger amplifications (e.g. Wambsganss & Paczynski 1991; Schneider, Ehlers, & Falco 1992).

Taking into account this characteristic of gravitational lens system (GLS), the radius of the broad line region (BLR), and a typical mass for the microlens (Alcock et al. 2000a,b), significant amplifications of the BEL would not be expected (Nemiroff 1988; Schneider & Wambsganss 1990). Then, GLS would not be a good tool to study the outer regions of AGNs.

However, according to more realistic studies about the sizes of the BLRs of quasars (Wandel, Peterson & Malkan 1999) based on the reverberation mapping method (Blandford & McKee 1982), the sizes of the BLRs were reduced in an order of magnitude. This motivates the revision of the influence of microlensing on

Send offprint requests to: C. Abajas

the different quasars emission regions (Abajas et al. 2002).

2. Microlensing by an isolated lens

2.1. Is there any quasar with $r_{\rm blr} \leq \eta_0$ among the known GLS ?

Is BEL microlensing possible in any of the known GLS? For a typical GL with $z_{lens} = 0.5$ and $z_{source} = 2$ an Einstein radius of around 20 light days is obtained. To know the size of the BLR the Kaspi et al. (2000) relationship between the BLR radius and the intrinsic luminosity of QSO, $r_{\rm blr} \propto L^{0.7}$, can be used. With this relationship and the NGC5548 system as reference, Abajas et al. (2002) found that a fraction of 30% GLS has a BLR radius for high ionization lines (HIL) between 1 and 10 lt-days, and an order of magnitude greater for low ionization lines (LIL). For example favorable systems to detect the effects of microlensing on the BEL are SDSS J1004+4112 and B1600+434, which have sizes of HIL region of half η_0 for $1 M_\odot$ microlens.

2.2. Models

The Einstein radius, η_0, projected into the source plane is:

$$\eta_0 = \sqrt{\frac{4GM}{c^2}\frac{D_{\rm s} D_{\rm ds}}{D_{\rm d}}} \quad (1)$$

where G is the gravitational constant, M is the mass of the star, c is the speed of light, and $D_{\rm d}$, $D_{\rm s}$ and $D_{\rm ds}$ are the angular diameter distances of the lens, source and from the lens to the source respectively.

Throughout the paper we will use the standard notation for gravitational lensing (Schneider, Ehlers, & Falco 1992). All distances are normalized to the Einstein radius associated with this microlens mass. A standard cosmology with $H_0 = 70$ kms^{-1}Mpc^{-1}, $\Omega_{\rm M} = 0.3$, and $\Omega_\Lambda = 0.7$ is considered.

We compute the emission-line profile from the expression

$$F_\lambda = \int_V \epsilon(r)\, \delta\left[\lambda - \lambda_0\left(1 + \frac{v_{\shortparallel}}{c}\right)\right] \mu(\boldsymbol{r})\, dV, \quad (2)$$

where we consider three different geometries (spherical, biconical, and cylindrical) and adopt the following radial dependences for the emissivity and magnitude of the velocity:

$$\epsilon(r) = \epsilon_0 \left(\frac{r}{r_{\rm in}}\right)^{\beta} \quad (3)$$

and

$$v(r) = v_0 \left(\frac{r}{r_{\rm in}}\right)^{p}. \quad (4)$$

The amplification associated with the point like microlens is:

$$\mu(\boldsymbol{r}) = \frac{u^2+2}{u\sqrt{u^2+4}} \quad \left(u = \frac{|\boldsymbol{r} - \boldsymbol{r}_0|}{\eta_0}\right) \quad (5)$$

being $\boldsymbol{r}_0 \sim (r_0, \varphi_0)$ the position of the microlens, η_0 the Einstein radius, and $v_{\shortparallel}$ is the projected line-of-sight velocity.

The transversal velocity in the different geometries are:

$$v_{\shortparallel} = \begin{cases} v(r)\, \cos\theta & \text{for spherical shell} \\ v(r)\, \xi_{\perp,\shortparallel} & \text{for biconical shell} \\ v(r)\, \cos\varphi \sin i & \text{for Keplerian disk} \end{cases} \quad (6)$$

being $p > 0$ except for the Keplerian disk ($p = -0.5$) and i the inclination of the system with respect to the line of sight. $\xi_\perp$ and $\xi_\shortparallel$ are the projections of the bicone when it turns around x and y axes respectively, being $\xi_\perp = \sin\theta \sin\varphi \sin i + \cos\theta \cos i$ and $\xi_\shortparallel = \sin\theta \cos\varphi \sin i + \cos\theta \cos i$. Both projections fit in when $i = 0°$.

In the modified Keplerian model the velocity is chosen so that the velocity is zero in the outer limit of the region, so then the profile have only one peak.

$$v(r) = v_0 \left(\frac{\frac{1}{r} - \frac{1}{r_{\rm blr}}}{\frac{1}{r_{\rm in}} - \frac{1}{r_{\rm blr}}}\right)^{-p} \cos\varphi \sin i, \quad (7)$$

being $p = -0.5$.

We adopt inner ($r_{\rm in}$) and outer ($r_{\rm BLR}$) radii for the BLR and it is assumed throughout that $r_{\rm in} = 0.1\ r_{\rm BLR}$. We consider two values (1 and 4) for $r_{\rm BLR}/\eta_0$. The emissivity law, β, is considered equal to -1.5.

To study the effects produced by the relative off-centering between the microlens and

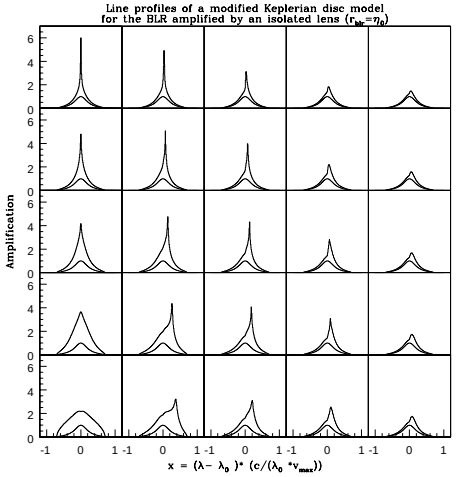

Fig. 1. Model of a modified Keplerian disk with $i = 45°$, $p = -0.5$, $\beta = 1.5$, and $r_{\rm blr} = \eta_0$. On the x-axis we represent the velocity. On the y-axis we represent the flux of the line profile. The heavy solid line is the amplified line profile, and the lighter solid line is the unamplified line profile.

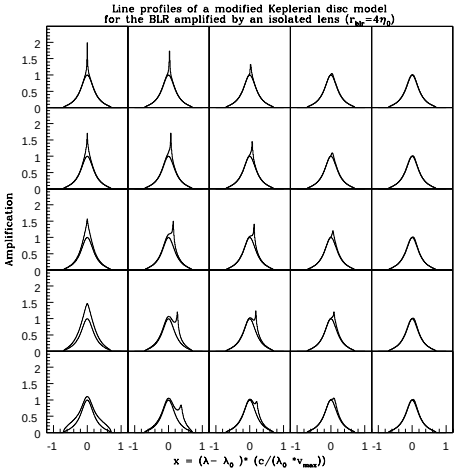

Fig. 2. Same as in Fig. 1, but for $r_{\rm blr} = 4\eta_0$.

the BLR, we compute line profiles corresponding to a grid of displacements of the microlens relative to the center of the BLR. We consider 25 positions in the positive XY quadrant ranging from 0 to $r_{\rm BLR}/\eta_0$ in both the X and Y axes. In Abajas et al. (2002) all the formal development, formulae and figures are collected. In each location a line profile is calculated (Figs. 1,2).

Fig. 1 has $r_{\rm blr} = \eta_0$ (i.e. if the BLR has 10 lt-days, the mass of the microlens is $0.25M_\odot$). Then the global amplification is very important when observer, lens and source are in the optical axis, but this effect decreases if the lens is placed far away. Other microlensing effects are the change of the line profile shape and the shift of the peak of the line. If this simulation is repeated using a less massive lens ($0.015M_\odot$ lens for a $r_{\rm blr} = 10$ lt-days), i.e. $r_{\rm blr} = 4\eta_0$, then we can observe in Fig. 2 that now the global amplification has disappeared even at the origin of the system, but the asymmetries and peak-shift are still visible. So it is possible to measure different redshifts from different images of the same system.

According to these results it would be possible to detect ML on Broad Emission Lines. The global amplification can be relevant, specially in HIL (of small sizes). In Abajas et al. (2002) a group of GLS for which ML effects can be potentially observed was identified. Differential amplification is easily detectable except for highly symmetric velocity fields. Line shifts are also expected.

3. Microlensing by a straight fold caustic

In most of cases we can not simply consider that microlensing is caused by an isolated compact object but we must take into account that the micro-deflector is placed in an extended object (tipically, the lens galaxy). In this case, an idealized situation of a straight fold caustic with infinite length passing over the disk can be considered. This is a crude but interesting approximation if the size of the source(i.e. disk) of interest is smaller than the Einstein-ring radius on the source plane. Then the following analytical approximated formula can be used for the amplification factor associated to a straight fold caustic (Chang

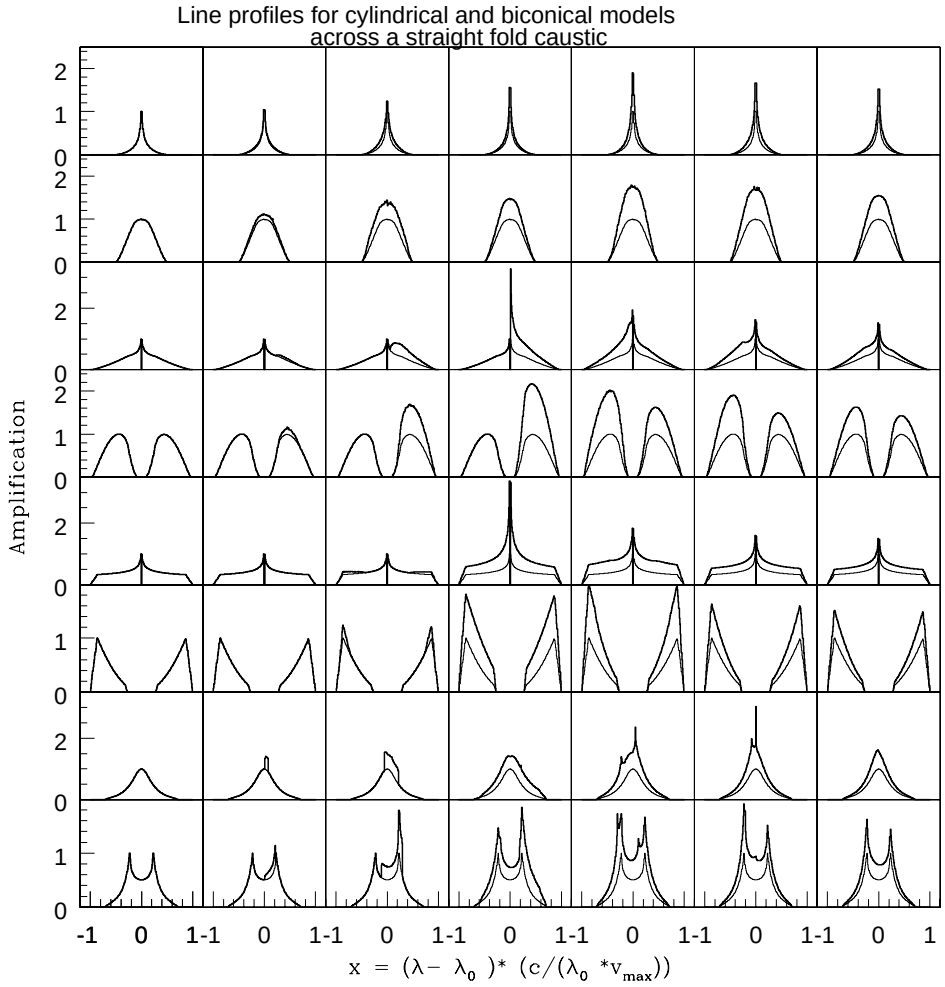

Fig. 3. The models run vertically, being from the bottom to the top Keplerian, modified Keplerian, and six biconical models with this pairs of (p, i): (0.5, 0°), (2, 0°), (0.5, 45°), (2, 45°), (0.5, 90°), (2, 90°). The different distances to the oblique straight fold caustic run horizontally. On the x-axis we represent the velocity. On the y-axis we represent the flux of the line profile. The heavy solid line is the amplified line profile, and the lighter solid line is the unamplified line profile.

& Refsdal 1984; Schneider, Ehlers, & Falco 1992):

$$\mu(\delta) = \begin{cases} A_0 + \frac{\epsilon}{\sqrt{\delta}} & \text{If } \delta > 0, \\ A_0 & \text{If } \delta < 0, \end{cases} \quad (8)$$

where δ is the separation from the caustic in units of η_0, A_0 is the amplification outside the caustic, and ϵ represents a constant amplification factor of order of unity, which depends on the crossing point on the caustic (Witt, Kayser & Refsdal 1993). We will assume $A_0 = 1$ and $\epsilon = 1$, although higher values will cause higher amplification.

To illustrate the effects of microlensing by a oblique straight fold caustic crossing in Fig. 3 we present as summary the cases corresponding to a Keplerian disk, a modified Keplerian disk and a bicone. As it can be seen in this fi-

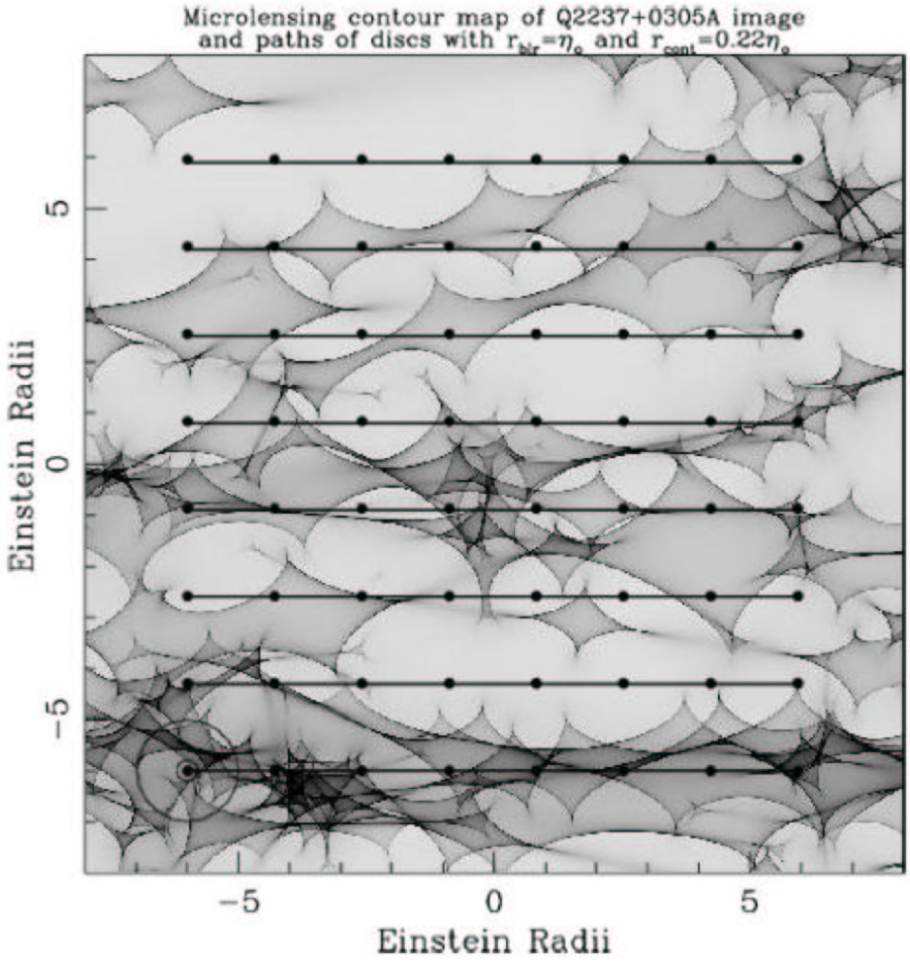

Fig. 4. The magnification map, $\mu(\boldsymbol{r})$, used here to calculate the changes on the shape of the line profile. The bigger circle represents the projected BLR, the smaller circle represents the projected continuum region, and points are the different positions over the magnification map.

gure (3) the results indicate that the effects of microlensing are also noticeable in this case. However, the straight fold caustic approximation is only valid when the source is very small as compared with the caustic. This hypothesis is not, in general, realistic for the BLRs and the study of complex magnification patterns induced by the granulation of the mass distribute in the lens galaxies is needed.

4. Microlensing by a caustic network

4.1. The BLR

Lewis & Ibata (2004) introduced the study of microlensing by a caustic network. They found that the BLR can be significantly amplified by the action of microlensing, although the degree of magnification depends upon the spatial and the kinematic structure of the BLR. Furthermore, while there is a correlation between the microlensing fluctuations of the con-

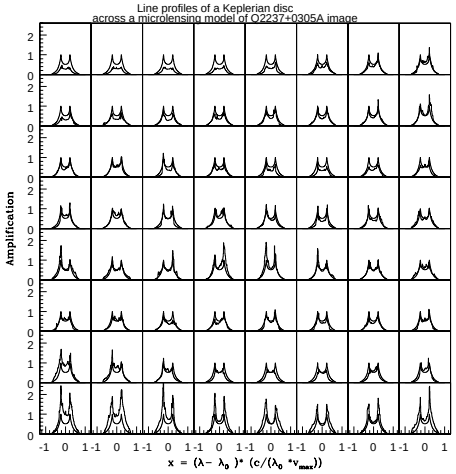

Fig. 5. Model of a Keplerian disk for the BLR with $i = 45°$, $p = -0.5$, $\beta = 1.5$ and $r_{\rm blr} = \eta_0$. On the x-axis we represent the velocity. On the y-axis we represent the flux. The heavy solid line is the amplified line profile, and the lighter solid line is the mean amplified line profile.

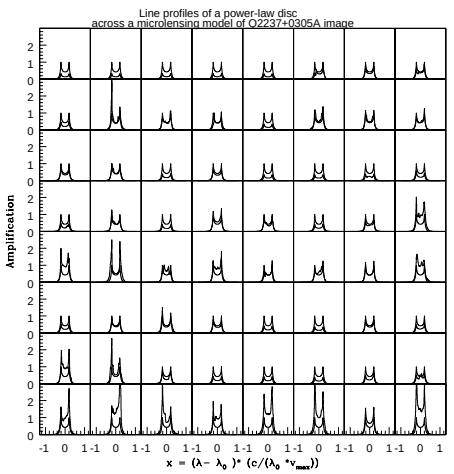

Fig. 6. Model of a Keplerian disk for the continuum with $i = 45°$, $p_{\rm ss} = 3/2$ and $r_{\rm cont} = 0.22\eta_0$. On the x-axis we represent the velocityv. On the y-axis we represent the flux. The heavy solid line is the amplified line profile, and the lighter solid line is the mean amplified line profile.

tinuum source and the BLR, there is a substantial scatter about this relation, revealing that broad-band photometric monitoring is not necessarily a guide to BEL microlensing.

Using the parameters for the mass density distribution, κ, and the shear, γ, of Schmidt, Webster, & Lewis (1998), and the inverse ray-shooting method (e.g. Schneider, Ehlers, & Falco 1992), we compute a magnification pattern for Q2237+0305A (Fig. 4), being $\kappa = 0.36$ and $\gamma = 0.40$.

To study the effects produced on the broad emission line corresponding to a Keplerian disk model by microlenses at high optical depth in the A image of Q2237+0305, we convolve the line profile with this magnification pattern in different positions, marked with points in Fig. 4. The amplification is significant for a number of position of projected disk. Notice that we also obtain slightly unamplified line profiles in some positions (Fig. 5).

4.2. Continuum

We assume a disk geometry for the region emitting the continuum radiation. We will suppose that this disk has uniform thickness, $h \ll r_{\rm in}$, and that the angle between its axis and the line of sight is i. Finally, any point in the disk is assumed to follow a circular orbit about the axis, giving a line-of-sight Keplerian velocity.

For this system, the amplified line profile is

$$F_\lambda = \int_S I_{\rm ss}(r)\, \delta\left[\lambda - \lambda_0\left(1 + \frac{v_\parallel}{c}\right)\right] \mu(\boldsymbol{r})\, dS, \quad (9)$$

where the brightness distribution of the continuum source is adopted as,

$$I_{\rm ss}(r) = 2^{p_{\rm ss}} I_{\rm ss}\left(1 + \frac{r^2}{R_{\rm ss}^2}\right)^{-p_{\rm ss}}, \quad (10)$$

with a power-law index $p_{\rm ss} = 3/2$, a typical intensity $I_{\rm ss} = I_{\rm ss}(R_{\rm ss})$ and a typical radius $R_{\rm ss} = R_{\rm ss}(90\%)(10^{1/(p_{\rm ss}-1)} - 1)^{1/2}$. This power-law model was chosen because it represents a rough version of the standard acretion disk model (Shalyapin et al. 2002).

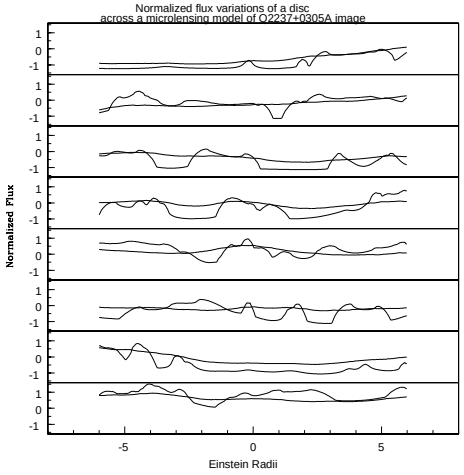

Fig. 7. Light curves of the BLR and the continuum represented in solid and lighter solid line, respectively. Each pair of light curves is computed across different paths drawn on Fig. 4.

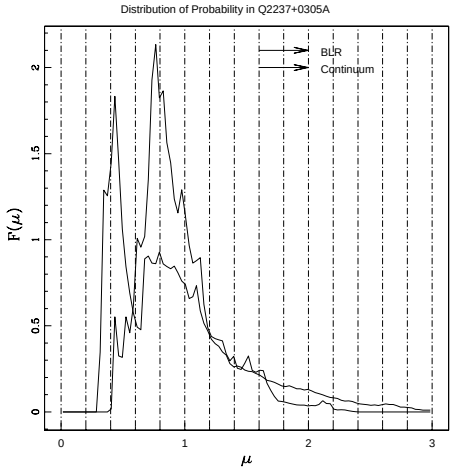

Fig. 9. Probability distribution of the magnification of the BLR, in solid line, and the continuum, in lighter solid line.

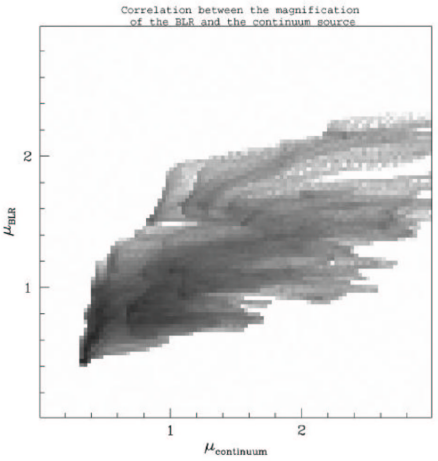

Fig. 8. The correlation between the magnification of the BLR and the continuum is represented, when a Keplerian model is considered for both sources.

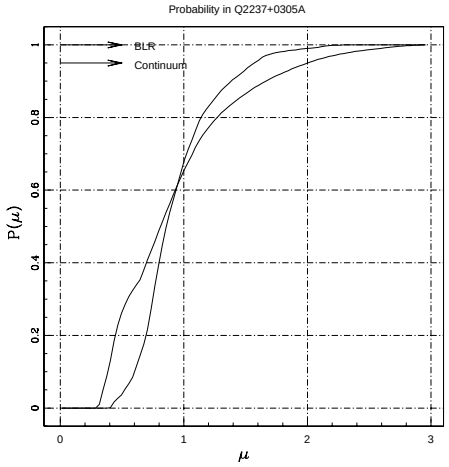

Fig. 10. Accumulate probability of the magnification of the BLR, in solid line, and the continuum, in lighter solid line.

We assume that the continuum radius is $r_{\rm cont} = 2.27$ lt-days, which means $r_{\rm cont} = 0.22\ \eta_0$.

Fig. 6 corresponds to the continuum Keplerian disk convolved with the magnification pattern in different positions, marked with points in Fig. 4.

The microlensing light curve of both sources, the BLR and the continuum, can be found by convolving the source profile with the magnification map at different positions across the source plane (thick lines in Fig. 4).

In Fig.7 the light curves for both the BLR and the continuum are shown, where $i = 45°$. This light curves correspond to the paths shown in Fig. 4. These curves are normalized to the mean amplification ot the pattern.

Fig. 7 indicates, in first place, that greater than a 10% changes could be detectable in the BEL. There is a global correlation between the BEL and continuum light curves although according to Lewis, & Ibata (2004) there is significant scatter around this mean behaviour. This can be better appreciated in Figures 8, 9 and 10, where the correlation between the BLR and the continuum, the probability distribution and the acummulated probabilities are represented.

5. Conclusions

The main conclusion is that ML events could modify the BEL from multiple imaged QSOs and AGNs. Although global amplification can be relevant in many cases, other effects like blue/red enhancements or line shifts can be more easy to recognize.

However, the observational world is more complex. For instance, the BLR and the NLR (narrow line region) are merged and GLS are compact and difficult to be observed. Spectra with high S/N at the wings profile, probably monitored using an Integral Field Spectrographs are needed.

In any case, BEL microlensing is a promising tool to test the modern ideas about the BLR size and stratification, that can open a new window to understand the physics of the BLR.

Acknowledgements. We are specially grateful to Rodrigo Gil-Merino for his inestimable help and worthwhile comments about the ray shooting method. This work was supported by the P6/88 project of the IAC and P1196 supported by the Ministry of Science of Serbia. L. Č. P. is supported by Alexander von Humboldt Foundation through "Rückkehrstipendium".

References

Abajas, C., Mediavilla, E., Muñoz, J. A., Popović, L. Č., & Oscoz, A. 2002, ApJ, 576, 640.
Alcock, C. et al. 2000a, ApJ, 541, 734
Alcock, C. et al. 2000b, ApJ, 542, 281
Blandford, R. D., & McKee, C. F. 1982, ApJ, 255, 419
Chang K., & Refsdal S. 1984, A&A 132,168
Kaspi, S. et al. 2000, ApJ, 533, 631
Lewis, G. F., & Ibata, R. A. 2004, MNRAS, 348, 24
Nemiroff, R. 1988, ApJ, 335, 593
Peterson, B. M., & Wandel, A. 1999, ApJ, 521, L95
Rees, M. 1984, ARA&A, 22, 471
Schneider, P., Ehlers, J., & Falco, E. 1992, Gravitational Lenses (Berlin: Springer)
Schneider, P., & Wambsganss, J. 1990, ARA&A, 273, 42
Schmidt, R., Webster, R. L., & Lewis, G. F. 1998, MNRAS, 295, 488
Shalyapin, V. N. et al. 2002, ApJ, 579, 127
Wandel, A., Peterson, B. M., & Malkan, M. A. 1999, ApJ, 526, 579
Wambsganss, J., & Paczynski, B. 1991, AJ, 102, 864
Witt, H. J., Kayser, R., & Refsdal, S. 1993, A&A, 268, 501